Zero-temperature generalized phase diagram of the 4*d* transition metals under pressure

C. Cazorla,[1,2,3] D. Alfè,[1,2,3,4] and M. J. Gillan[1,2,3]
[1]*London Centre for Nanotechnology, UCL, London WC1H OAH, United Kingdom*
[2]*Department of Physics and Astronomy, UCL, London WC1E 6BT, United Kingdom*
[3]*Materials Simulation Laboratory, London WC1E 6BT, United Kingdom*
[4]*Department of Earth Sciences, UCL, London, WC1E 6BT, United Kingdom*
(Received 13 March 2008; published 4 June 2008)

We use an accurate implementation of density-functional theory to calculate the zero-temperature generalized phase diagram of the 4*d* series of transition metals from Y to Pd as a function of pressure *P* and atomic number *Z*. The implementation used is full-potential linearized augmented plane waves, and we employ the exchange-correlation functional recently developed by Wu and Cohen. For each element, we obtain the ground-state energy for several crystal structures over a range of volumes, the energy being converged with respect to all technical parameters to within ~1 meV/atom. The calculated transition pressures for all the elements and all transitions we have found are compared with experiment wherever possible, and we discuss the origin of the significant discrepancies. Agreement with experiment for the zero-temperature equation of state is generally excellent. The generalized phase diagram of the 4*d* series shows that the major boundaries slope toward lower *Z* with increasing *P* for the early elements, as expected from the pressure induced transfer of electrons from *sp* states to *d* states, but are almost independent of *P* for the later elements. Our results for Mo indicate a transition from body-centered cubic to face-centered cubic, rather than the bcc-hcp transition expected from *sp*-*d* transfer.

DOI: 10.1103/PhysRevB.77.224103 PACS number(s): 61.50.Ks, 61.50.−f, 61.43.Bn

I. INTRODUCTION

The transition metals are among the most intensively studied families of elements, and there has been an effort going back several decades to map and interpret systematic trends in their properties. Some of these trends are of fundamental importance to our understanding of the energetics and electronic structure of transition metals. Examples include: the parabolic dependence of cohesive energy and bulk modulus on *d*-band filling;[1] the sequence of most stable crystal structures associated with increasing band filling at ambient pressure;[2] and the pressure induced increase of *d*-band width going roughly as the fifth inverse power of the atomic volume.[3] However, our knowledge of transition-metal systematics is still very far from complete, as is evident from the current major controversies over high-pressure melting curves.[4–7] Even at low temperatures, there are sizable gaps in the map of transition-metal phase diagrams, and new crystal structures continue to be discovered.[8] We report here a systematic investigation of the zero-temperature phase diagram of all the 4*d* transition metals over a wide range of pressures, based on one of the most accurate implementations of density-functional theory (DFT) currently available.

There have, of course, been very many previous detailed studies of transition metals based on DFT, some of which investigated the relative stability of different crystal structures at high pressures. However, most previous work has been designed to address particular questions relating to particular metals. Here, by constrast, the aim is to obtain a coherent overall view of an entire transition-metals series. Specifically, using *Z* to denote atomic number, we wish to use DFT to map out the generalized (P,Z) phase diagram of the 4*d* series at $T=0$ K at pressures *P* up to ~500 GPa.[9] In order to substantiate the accuracy of the calculations, we shall compare our calculated results for *P* as a function of volume *V* with all available experimental data. The calculations are all performed using the full-potential linearized augmented plane waves[10–13] (FP-LAPW) implementation of DFT, which for a given exchange-correlation functional is among the most accurate ways of calculating the total energy. We use the exchange-correlation functional recently developed by Wu and Cohen,[14] which appears to reproduce the experimental energetics of 4*d* transition metals more accurately than other functionals.[15]

There are several motivations for wishing to obtain the (P,Z) phase diagram of a transition-metal series at $T=0$ K. One motivation is the possibility of discovering hitherto unknown crystallographic phase boundaries for particular metals. Another motivation is to probe our basic understanding of transition-metal energetics. At ambient pressure, the most stable crystal structures of the 4*d* and 5*d* series follow the sequence hexagonal close packed (hcp) to body-centered cubic (bcc) to hcp to face-centered cubic (fcc) with increasing *Z*, and the 3*d* series nearly follows this sequence, the deviations being caused by magnetic effects.[16,17] This sequence is entirely explained by band energies, and can be reasonably well reproduced using a canonical *d*-band tight-binding model with some modifications due to hybridization with *sp* bands.[18–20] The main effect of pressure is to shift the relative energies of the *d*-band centroid and the bottom of the *sp* band, and hence increase the *d*-band filling.[18] This leads one to expect that the same sequence of structures will be found at high *P*, but with the boundaries shifted to the left (toward lower *Z*).[21,22] We shall confirm that this is the case, though the reality is slightly more complicated.

In addition to the motivations we have mentioned, there is another that is important to us. Current controversies over the high-pressure melting curves of transition metals stem from apparent disagreements between melting temperatures

deduced from static compression and shock experiments, these disagreements amounting to several thousand Kelvin at megabar pressures.[6,7] DFT calculations of transition-metal melting curves[4,5,23] support the correctness of the shock results, and one of the proposed resolutions of the conflicts is that the transitions identified as melting in static compression are in fact solid-solid transitions. It would clearly help to reduce the confusion if we had a better understanding of the generalized (P,T,Z) phase diagram of transition-metal series.[9] At present, we have a fairly complete knowledge of this only at low P, and, to a lesser extent, at low T. We see the present attempt to complete the low-T (P,Z) diagram as an essential step toward mapping the full (P,T,Z) diagram.

Earlier DFT work has already given much information about the energetics of transition metals at $T=0$ K. Particularly important here is the work of Pettifor[18,24,25] and others, which provided a systematic understanding of the structural trends across all the transition-metal series in terms of the electronic densities of states of different crystal structures. Their work also gave important insights into the pressure induced transfer of electrons from sp states to d states. Also important was the first-principles work of Skriver[26] on structural trends across transition-metal series at zero pressure. The pioneering work of Moriarty, Johansson, and others on the high-pressure energetics of transition metals will be cited below. The information from all this previous work could be assembled to produce a substantial part of the (P,Z) diagram, but there would be inconsistencies from the use of different DFT implementations and exchange-correlation functionals. Here, we avoid such inconsistencies by using a single high-accuracy method for all the calculations.

The remainder of the paper is organized as follows. In Sec. II, we summarize the essential ideas underlying the methods used in this work and the results of our convergence tests. Then (Sec. III), we present for each of the transition metals from Y to Pd our calculated energy differences between different crystal structures and the equation of state (EOS) $P(V)$ for pressures from ambient to ~ 500 GPa, comparing our results to experiments and previous calculations where possible. At the end of Sec. III, we present the zero-temperature (P,Z) phase diagram of the $4d$ transition-metal series. Discussion and conclusions are in Sec. IV.

II. TECHNIQUES AND TESTS

There are several implementations of DFT that can be used to calculate the total energy per atom of a crystal, including pseudopotential techniques,[27] the projector augmented wave technique,[28,29] the full-potential augmented plane-wave technique,[10–13] etc. We have chosen to use FP-LAPW here because for a given exchange-correlation functional, it can give values for the total energy that are closer to the exact value than most other implementations. There are a number of technical parameters in FP-LAPW that control convergence toward the exact value. We recall in this section the main ideas of FP-LAPW, summarize the parameters that control convergence, and report tests that guide our setting of these parameters. The exchange-correlation functional used for all the present work is that due to Wu and Cohen.[14] Later in this section, we outline briefly what this functional is, and we report tests indicating that it should be particularly accurate for present purposes.

A. Full-potential linearized augmented plane waves

In APW methods, space is divided into nonoverlapping muffin-tin spheres (radius R_{MT}) centered on the atoms and the interstitial region between the spheres. Each Kohn-Sham orbital is represented as a sum of radial functions multiplied by spherical harmonics up to a maximum angular momentum $l_{\mathrm{orb}}^{\mathrm{max}}$ in each sphere, and as a sum of plane waves (maximum wave vector K_{max}) in the interstitial region; the coefficients are adjusted to achieve continuity at the sphere boundaries. The Kohn-Sham eigenstates are divided into core and valence states; core states are treated as being nonzero only inside the muffin-tin spheres, while valence states extend over all space. The radial functions used as basis sets are solutions of the Schrödinger equation inside the atomic spheres, and are therefore energy dependent. In LAPW, the energy dependence is treated in a linear approximation. In full-potential implementations (FP-LAPW), the Kohn-Sham potential is also represented as a sum over angular-momentum functions within the spheres (maximum angular momentum $l_{\mathrm{pot}}^{\mathrm{max}}$) and a sum over plane waves (maximum wave vector G_{max}) in the interstitial region. As it stands, this scheme is not accurate if there are semicore states, i.e., low-lying states that are not adequately treated by linearization. One solution to this problem is to linearize the basis functions using different reference energies for valence and semicore states. Alternatively, one can augment the basis set with "local orbitals," this procedure being known as the "APW +lo" method. We use the full-potential version of the latter method here in order to treat all the valence and semicore states. A fully relativistic treatment is used for core states, and a scalar relativistic treatment for all other states. The wave vectors $\mathbf{k}$ for which the Kohn-Sham equations are self-consistently solved must be sampled over the Brillouin zone of the crystal, and the well-known Monkhorst-Pack k-point sampling scheme is used for this purpose.[30] All the calculations were performed using the WIEN2k code.[31]

Throughout the present calculations, we aim to achieve convergence of the total energy to within 1 meV/atom with respect to all the parameters we have just mentioned. All states having principal quantum number $n \leq 3$ are treated as core states, and all higher states as valence states. This choice is based on the fact that the states with $n=3$ lie at least 200 eV below the Fermi level so they will not respond significantly to compression even at megabar pressures. Provided the muffin-tin spheres do not overlap, and provided the calculations are fully converged with respect to all parameters, the choice of R_{MT} should not affect the results, but it does affect the efficiency of the calculations. We used the default setting of R_{MT} provided by the WIEN2k algorithm, which ensures that R_{MT} varies appropriately as the volume per atom is varied (that is, keeping the ratio between the unit cell and muffin-tin sphere volumes more or less constant). To determine the settings required for the technical parameters K_{max}, G_{max}, $l_{\mathrm{orb}}^{\mathrm{max}}$, and $l_{\mathrm{orb}}^{\mathrm{pot}}$, and for k-point sampling, we have

TABLE I. Tests on convergence of FP-LAPW total energy per atom E_{tot} (eV units) for bcc Mo. Variation of E_{tot} is reported with respect to k-point sampling, plane-wave cutoff G_{max} (bohr^{-1} units) and angular-momentum cutoff l_{pot}^{max} in representation of Kohn-Sham potential, and plane-wave cutoff K_{max} and angular-momentum cutoff l_{orb}^{max} in representation of orbitals (R_{MT} is muffin-tin radius). In each section of the Table, only a single parameter is varied, the other parameters being fixed as $14\times14\times14$ (k-point sampling), $G_{max}=18$ bohr^{-1}, $l_{pot}^{max}=4$, $R_{MT}K_{max}=9.5$ and $l_{orb}^{max}=10$.

k points	E_{tot}
$10\times10\times10$	−110178.7071
$14\times14\times14$	−110178.7100
$16\times16\times16$	−110178.7089
$18\times18\times18$	−110178.7095
G_{max} (bohr^{-1})	E_{tot}
14	−110178.7099
18	−110178.7100
20	−110178.7100
l_{pot}^{max}	E_{tot}
4	−110178.7100
6	−110178.7100
$R_{MT}K_{max}$	E_{tot}
8.0	−110178.6681
9.0	−110178.7044
9.5	−110178.7100
10.5	−110178.7102
l_{orb}^{max}	E_{tot}
10	−110178.7100
12	−110178.7093

conducted systematic tests on bcc, fcc, and hcp Mo; we assume that the settings that give the required accuracy for Mo will also serve for all the 4d transition metals in all the structures of interest.

Our tests on Mo indicate that the choices $R_{MT}K_{max}=9.5$, $G_{max}=18$ bohr^{-1}, $l_{orb}^{max}=10$, and $l_{pot}^{max}=4$, together with $14\times14\times14$ k-point sampling ($14\times14\times7$ for hcp), give convergence to within ~1 meV/atom. To demonstrate that this is the case, we have set all of these parameters except one to the values just quoted, and studied the effect of varying the free parameter. The values of total energy per atom E_{tot} obtained when we vary in turn $R_{MT}K_{max}$, G_{max}, l_{orb}^{max}, l_{pot}^{max}, and k-point sampling are reported in Table I, from which we see that the required convergence is indeed achieved with the quoted values. These are the values used for all the calculations reported later. We note that, although we have paid careful attention to convergence, there remain small errors due to the linearization inherent in the FP-LAPW scheme.

B. Wu-Cohen exchange-correlation functional

The Wu-Cohen (WC) exchange-correlation functional is a particular form of generalized gradient approximation (GGA). In GGAs, the total exchange-correlation energy is the integral over the volume of the system of a density of exchange-correlation energy, this density being expressed in terms of the number density $n(\mathbf{r})$ of electrons as $n(\mathbf{r})\epsilon_{xc}[n(\mathbf{r}),s(\mathbf{r})]$. Here, ϵ_{xc}, the exchange-correlation energy per electron at position $\mathbf{r}$, depends not only on $n(\mathbf{r})$ itself but also on the magnitude of its dimensionless gradient $s(\mathbf{r})=|\nabla n|/[2(3\pi^2)^{1/3}n^{4/3}]$. The energy ϵ_{xc} is expressed as $\epsilon_{xc}[n(\mathbf{r}),s(\mathbf{r})]=\epsilon_x^{unif}[n(\mathbf{r})]F_{xc}[n(\mathbf{r}),s(\mathbf{r})]$, where $\epsilon_x^{unif}(n)$ is the exchange energy per electron in the uniform electron gas of density n, and F_{xc} is the so-called enhancement factor.

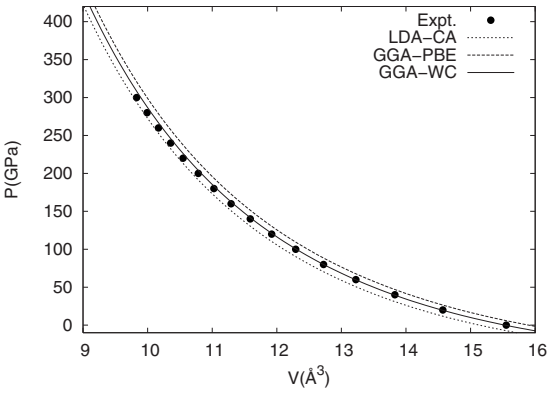

FIG. 1. Zero-temperature equation of state of Mo up to $P\sim400$ GPa calculated with GGA(WC), GGA(PBE) and LDA(CA) exchange-correlation functionals. Dots show experimental data.[36]

In the widely used Perdew-Burke-Ernzerhof (PBE) form of GGA,[32] a parameter-free formula expressing the dependence on s of $F_{xc}(s)$ was derived by requiring that certain exact conditions be satisfied. The WC functional takes the same GGA form as PBE for the correlation part of F_{xc}, but modifies the exchange part. The modification was done with the intention of improving the functional for condensed matter, at the expense of a somewhat worse description of atoms and molecules. Specifically, the modification was based on the idea that the exchange part of F_{xc} should be constructed so as to reproduce the fourth-order gradient expansion of the exact exchange-energy functional of the electron gas in the limit of slowly varying density.[34] The detailed form of the exchange enhancement factor in the WC functional can be found in the original paper,[14] which also presents the results of tests suggesting that the functional gives better results than LDA and PBE for the equilibrium lattice parameter and bulk modulus of a range of materials. Subsequently, tests of WC were reported on a much more extensive set of materials using the FP-LAPW implementation of DFT.[15] These tests supported the claim that WC is on average more accurate than LDA or PBE, but they showed that the improvement over these other functionals is by no means uniform. However, for 4d transition metals at ambient pressure, the WC predictions of equilibrium lattice parameter and bulk modulus are, with a few exceptions, better than both PBE and LDA.

To confirm that the quality of WC is maintained at high pressures, we compare in Fig. 1 our calculated results for pressure P as a function of volume V at zero temperature for Mo obtained with WC, LDA (Ceperley-Alder),[35] and PBE

with experimental results up to $P=300$ GPa. The experimental measurements were performed at room temperature but were corrected for thermal effects so that they refer to $T=0$ K.[36] The comparisons show that WC is in almost perfect agreement with experiment over the entire pressure range, while both LDA and PBE show significant deviations. Comparisons of calculated $P(V)$ curves with experimental data for other 4*d* transition metals presented in the Sec. III further confirm the quality of WC.

III. RESULTS

For each of the 4*d* transition metals from Y to Pd, we have calculated the total energy at a closely spaced series of atomic volumes for the body-centered cubic, face-centered cubic, and hexagonal close-packed structures. In some cases, we have also studied other crystal structures. For the case of noncubic structures, we optimize the corresponding c/a ratios once for some volume near equilibrium and then perform the calculations at fixed c/a ratio. However, in the presence of a phase transition, we reoptimize the c/a ratios of interest as required. The pressure as a function of volume is obtained for each structure by fitting the total energy results with a third-order Birch-Murnaghan equation of state.[37] From these results, we straightforwardly obtain the most stable crystal structure at each pressure, as well as the pressures of the structural transitions and the volumes of the coexisting phases at these transitions. In the following, we present first for each element the difference between the energy per atom in each structure and the energy in bcc structure, as a function of V. We then present $P(V)$ of the stable structures over the pressure range from ambient to typically 500 GPa. Where possible, we compare $P(V)$ and the transition pressures with experimental measurements, and we indicate the relation with previous theoretical results.

A. Yttrium

Experimentally, Y has the hcp structure at ambient pressure, and with increasing pressure passes successively to the α-samarium (αSm), double hcp (dhcp), and fcc structures.[38–40] This is the same sequence of structures observed in the lanthanides under pressure, as has often been discussed.[41] Earlier DFT calculations on Y have correctly predicted these structures,[42] and also indicated a transition to bcc at very high pressure.[43] Figure 2 reports our calculated energies of the hcp, αSm, dhcp, and fcc structures relative to bcc as a function of V. This shows the sequence of stable structures in the experimentally observed order. The resulting EOS is reported in Fig. 2 (we find $V_0=30.89$ Å^3/atom), and the transition pressures and volumes are given in Table II. Although the calculated sequence of crystal structures is the same as that observed experimentally, we significantly underestimate the transition pressures by at least 10 GPa. The difference is considerably greater for the transition αSm $\rightarrow$dhcp, but it is clear from Fig. 2 that the energy curves of these two structures follow each other so closely that the prediction of this transition pressure is likely to be very challenging. Possible reasons for our underestimation of the transition pressures are discussed in Sec. IV.

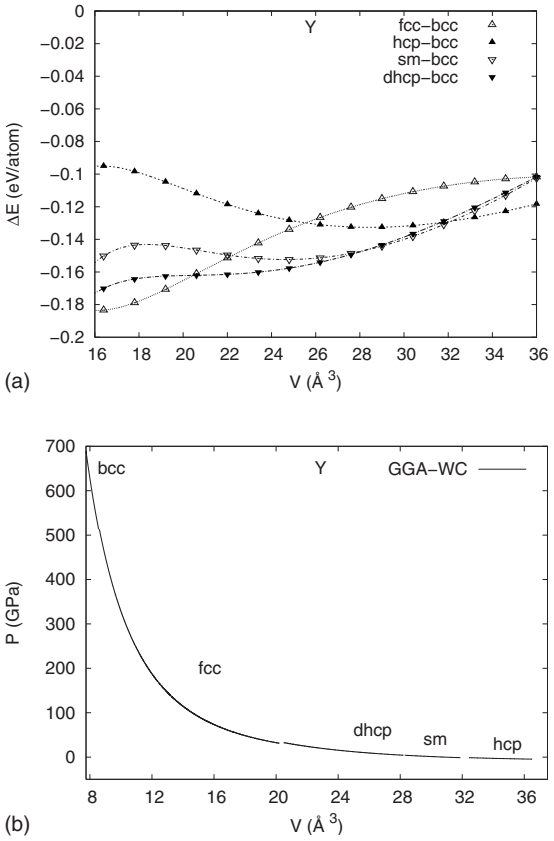

FIG. 2. *Top*: Energy differences ΔE of the hcp, αSm (C19), dhcp ($A3'$) and fcc structures with respect to bcc in Y as function of volume per atom. *Bottom*: Equation of state of Y up to $P \sim 700$ GPa.

We also report in Table II the results of very recent DFT work on Y up to $\sim$150 GPa by Lei *et al.*,[42] as well as those of the older work of Melsen *et al.*[43] The hcp-αSm and αSm-dhcp transition pressures P_t of Lei *et al.*, who used FP-LAPW based on LDA, are within 2 GPa of ours. It is known that some tranverse phonons of fcc Y are unstable at pressures below 90 GPa.[44] Based on this fact, Lei *et al.* analyze a distorted fcc structure that they find to be more stable than fcc. In order to save effort, however, we consider here the fcc structure directly. It is striking that the fcc-bcc P_t of Melsen *et al.*, obtained from FP-LMTO calculations based

TABLE II. Calculated volumes V_1, V_2 (units of Å^3/atom), and transition pressures P_t (units of GPa) from present work (earlier DFT results in parentheses), and experimental P_t for structural phase transitions in Y.

Transition	V_1	V_2	P_t DFT	P_t Expt.
hcp-αSm	32.44	31.88	−1.3 (−3 [a])	∼15 [c]
αSm-dhcp	28.30	28.21	4.2 (3 [a])	∼30 [c]
dhcp-fcc	20.49	20.32	32.7	∼44 [d]
fcc-bcc	8.61	8.57	513 (283 [b])	

[a]Reference 42 (LDA).
[b]Reference 43 (LDA).
[c]Reference 39.
[d]Reference 40.

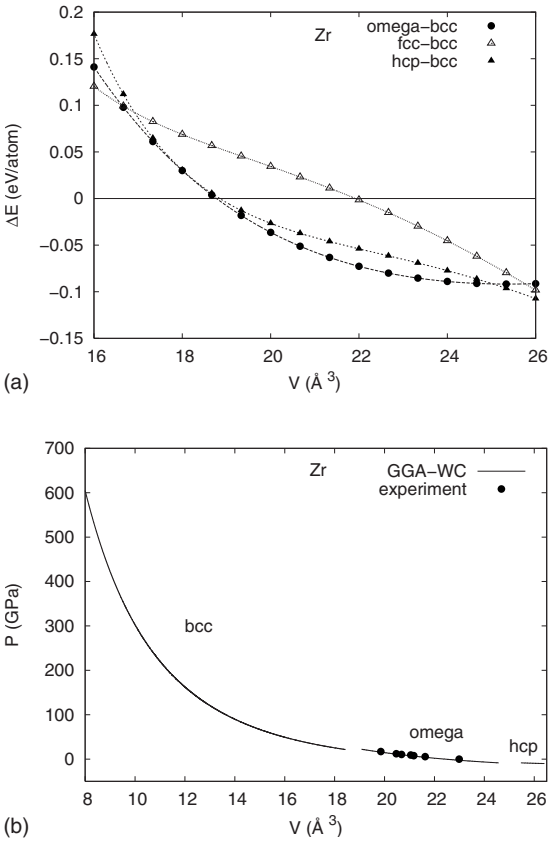

FIG. 3. *Top*: Energy differences ΔE of the hcp, ω (C32), and fcc structures with respect to bcc in Zr as function of volume. *Bottom*: Equation of state of Zr up to $P \sim 600$ GPa; dots represent experimental data from Ref. 45.

on LDA is below ours by over 200 GPa. It appears to us that their treatment of semicore states was much more approximate than the one used here, and this may account for the large difference. The very small volume change of only ~ 0.04 Å^3/atom that we find for this transition will magnify the effect of any technical errors in the prediction of P_t. We return to this question in Sec. IV.

B. Zirconium

Experimentally, the stable structure of Zr at ambient pressure is hcp, but measurements show a transition to the ω phase at the rather low pressure of 2.8 GPa, followed by a transition to bcc at $P \simeq 30$ GPa.[45] Our calculated energies of the ω, hcp and fcc structures relative to bcc as a function of volume (Fig. 3) show the same sequence, and our calculated $P(V)$ in the ω structure is in close agreement with experimental data. However, as in the case of Y, our calculations appear to underestimate the transition pressures (see Table III). We find that at $P=0$, $T=0$, the ω structure is most stable (with $V_0=23.04$ Å^3/atom and $c/a=0.62$), the transition between hcp and ω occurring at the negative pressure of -4.1 GPa. Our calculated transition pressure between ω and bcc of 22.2 GPa is also significantly below the experimental value of 30(2) GPa.[46] The underestimation by ~ 10 GPa is similar to what we found for Y, and will be discussed in Sec. IV.

Previous theoretical estimates of the ω-bcc transition pressure P_t show considerable variation (Table III). It seems that P_t from LDA is lower than that from PBE by ~ 10 GPa, but there are significant differences between results obtained with the same DFT functional. The results of Jona and Marcus[49] seem to be seriously out of line with both experiment and other calculations. We shall comment further in Sec. IV.

C. Niobium

Experimentally, the observed structure of Nb is bcc over the entire pressure range from ambient to ~ 145 GPa. Our total-energy results (Fig. 4) show that hcp, fcc, and ω are all less stable than bcc by at least 0.2 eV/atom over the pressure range up to over 400 GPa. A possible phase transition at pressures above 400 GPa may be suggested by the down-turn in the energy difference between hcp and bcc at ~ 400 GPa, but we have not pursued this possibility. The agreement of our calculated $P(V)$ curve with the recent experimental data of Kenichi and Singh[52] obtained at room temperature is excellent. Our calculated equilibrium volume V_0

TABLE III. Calculated volumes V_1, V_2 (this work, units of Å^3/atom), and calculated and experimental transition pressures P_t (units of GPa) for structural transitions in Zr. Calculated P_t values are listed according to the exchange-correlation function (WC, LDA or PBE) used.

			P_t (DFT)			
Transition	V_1	V_2	WC	LDA	PBE	P_t (expt.)
hcp-ω	24.45[a]	24.02[a]	−4 [a]			3[b]
ω−bcc	19.07[a]	18.43[a]	22[a]	24[c]	32[c]	30[d]
	21.61[e]	20.96[e]		16[f]	28[f]	
				5[g]		
				18[h]	29[h]	

[a]Present work.
[b]Reference 45.
[c]Reference 47.
[d]Reference 46.
[e]Reference 50 (LDA).
[f]Reference 48.
[g]Reference 49.
[h]Reference 51.

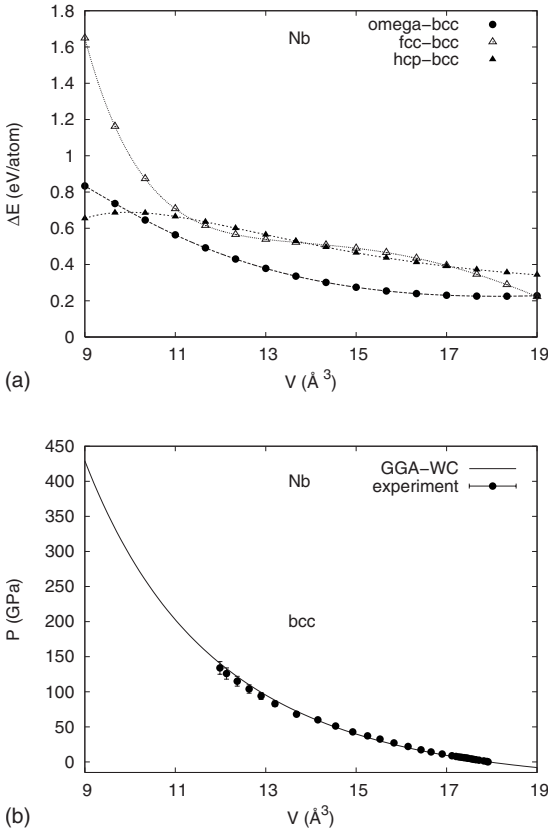

FIG. 4. *Top*: Energy differences ΔE of the ω, hcp, and fcc phases with respect to bcc in Nb as function of volume. *Bottom*: Calculated EOS of Nb compared to experimental data of Ref. 52.

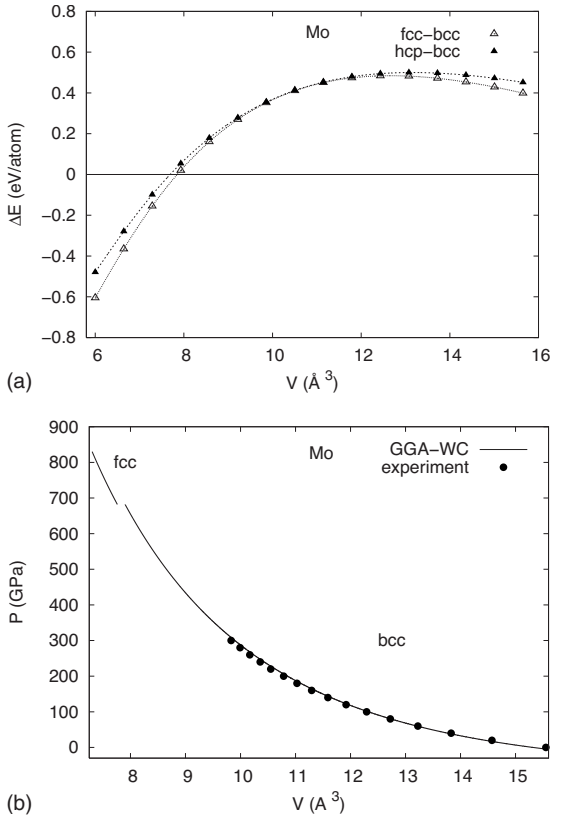

FIG. 5. *Top*: Energy differences ΔE of the fcc and hcp phases with respect to bcc in Mo as function of volume. *Bottom*: Equation of state of Mo compared with experimental data.[36]

$=17.94$ Å^3/atom agrees closely with the experimental value at ambient conditions[53] of 17.98 Å^3/atom.

D. Molybdenum

The properties of Mo have been intensively studied both experimentally and theoretically over the last decade. We mentioned in Sec. I the continuing controversy over its high-pressure melting curve. At low temperatures, experiments show that Mo has the bcc structure for all pressures up to ~400 GPa. There have been at least seven previous DFT studies on its phase transitions at higher pressures, and all agree that there is a transition to either hcp or fcc, but there is no consensus about which high-P form is more stable. There is also considerable variation of the predicted transition pressures. Our calculated energy differences fcc-bcc and hcp-bcc (Fig. 5) show clearly that bcc is the stable phase up to a pressure of nearly 660 GPa. Above this, both fcc and hcp fall below bcc, but fcc is below hcp, and the fcc-hcp difference becomes more negative with increasing pressure. Our calculated $P(V)$ curve is in excellent agreement with experimental data over the whole pressure range up to 300 GPa for which there are data (we find $V_0=15.53$ Å^3/atom).[36]

We summarize in Table IV all the DFT calculations on the high-P transition in Mo, noting the predicted high-P structure and transition pressure P_t to that structure, together with the DFT implementation and exchange-correlation functional. In general, we believe that work in which careful attention has not been give to convergence with respect to all technical parameters and the treatment of semicore states must be regarded as less reliable. However, it remains difficult to draw conclusions about the causes of the very large differences between predictions, in some cases based on exactly the same exchange-correlation functional. Further comments will be made in Sec. IV.

TABLE IV. DFT predictions of the high-pressure phase of Mo, with DFT method and exchange-correlation functional used, and transition pressure P_t (GPa units) from works cited in first column. Forms of LDA are due to Hedin-Lundqvist (Ref. 60) (HL), Perdew-Zunger (Ref. 61) (PZ) and von Barth-Hedin (Ref. 62) (BH), and of GGA to Perdew-Wang (Ref. 33) (PW) and Wu-Cohen (Ref. 14) (WC); the form of GGA used by Jona and Marcus was unspecified.

Ref.	High-P phase	DFT Method	E_{xc}	P_t
21	hcp	LMTO-ASA	LDA(HL)	420
58	hcp	FP-LMTO	LDA(HL)	520
59	hcp	FP-LMTO	LDA(PZ)	620
55	hcp	FP-LAPW	GGA(?)	620
56	fcc	FP-LMTO	LDA(BH)	580
57	fcc	LCGTO-FF	LDA(HL)	660
23	fcc	PAW	GGA(PW)	720
This work	fcc	FP-LAPW	GGA(WC)	660

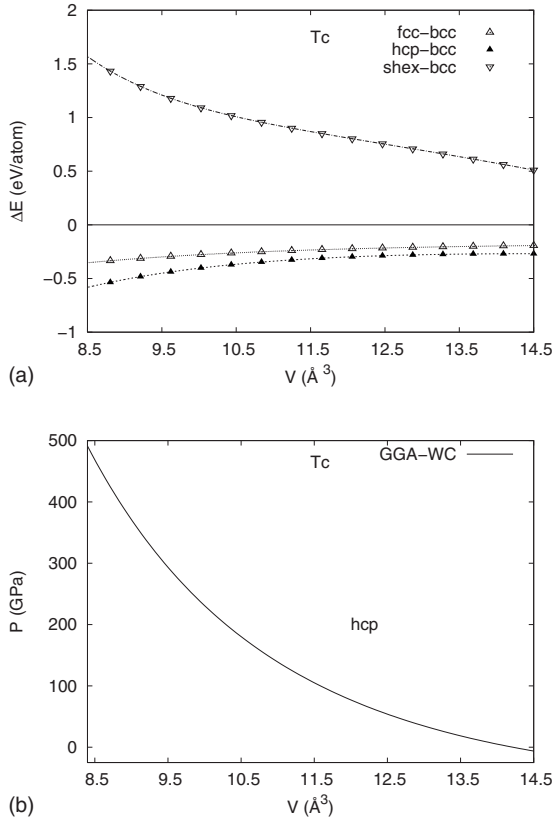

FIG. 6. *Top*: Energy differences ΔE of the fcc, hcp, and simple hexagonal (A_f) structures with respect to bcc in Tc as function of volume. *Bottom*: Equation of state of Tc up to 500 GPa.

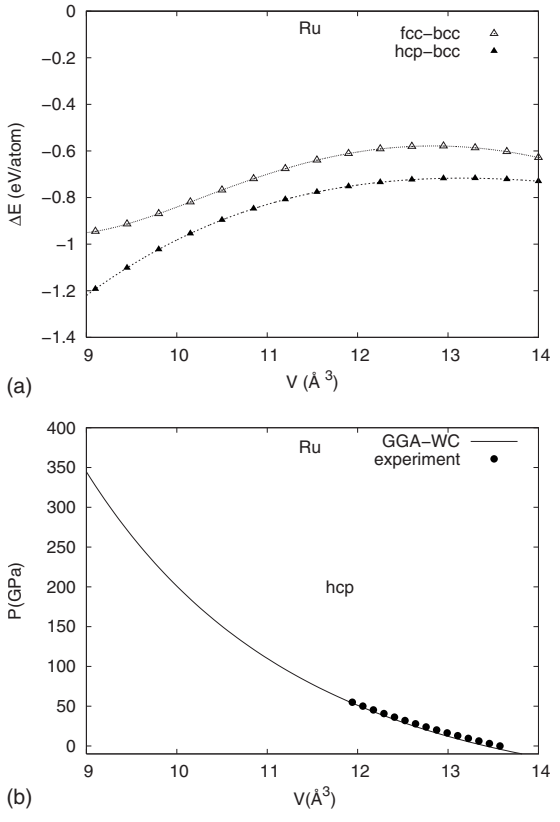

FIG. 7. *Top*: Energy differences ΔE of the hcp and fcc structures with respect to bcc in Ru as function of volume. *Bottom*: Equation of state of Ru up to $P \sim 400$ GPa compared with experimental data.[64]

E. Technetium

Tc has the hcp structure at ambient pressure, but little seems to be experimentally known about its behavior under pressure. Our results for the energies of the fcc, hcp, and simple hexagonal structures relative to bcc (Fig. 6) show that hcp is the most stable up to pressures of at least 500 GPa, and there is no indication that any of the other structures will become more stable at higher pressures than this. The calculated $P(V)$ curve of hcp Tc is reported in Fig. 6, but there appear to be no experimental data to compare it with. Our value for the equilibrium volume of 14.21 Å^3/atom (being $c/a=1.63$) agrees closely with the experimental value[63] 14.26 Å^3/atom.

F. Ruthenium

At ambient pressure, the structure of Ru is hcp. Experiments have been performed up to 56 GPa, and no phase transition has been found. Our results for the energies of the fcc and hcp structures relative to bcc (Fig. 7) show that hcp is the most stable up to pressures of at least 400 GPa. As can be seen in Fig. 7, our calculated EOS of hcp Ru is in very good agreement with recent experimental data.[64] In particular, we obtain an equilibrium volume of 13.42 Å^3/atom, which is close to the experimental value[65,66] of 13.47 Å^3/atom. (An earlier measured equilibrium volume[67] of 13.57 Å^3/atom is in rather poor agreement with our value.) We also note that our calculated c/a value of 1.58, which is similar to the result 1.57 obtained by Zheng-Johansson *et al.*[68] within LDA is exactly the value found experimentally.[64]

G. Rhodium and palladium

The last two elements treated here, Rh and Pd, both have the fcc structure at ambient pressure, and retain this structure up to the highest pressures reached so far experimentally[69,70] ($\sim$50 and 77.4 GPa, respectively). Our results for the energy differences fcc-bcc and hcp-bcc (Figs. 8 and 9) give no indication that any phase transition will be found in the range up to $\sim$500 GPa. As for most of the other 4*d* elements, our calculated EOS results (Figs. 8 and 9) are in close agreement with experiment. Our calculated equilibrium volumes of 13.71 and 14.73 Å^3/atom for Rh and Pd, respectively, agree closely with the experimental values[69,70] of 13.75 and 14.72 Å^3/atom.

H. Zero-temperature phase diagram

The pressures of the transitions for each element (atomic number Z) reported above can be regarded as points on phase boundaries drawn in the (P,Z) plane. These boundaries are described by the dependence of P on Z treated as a continuous, rather than a discrete variable. In the real world, the elements form a discrete series, and only integer values of Z

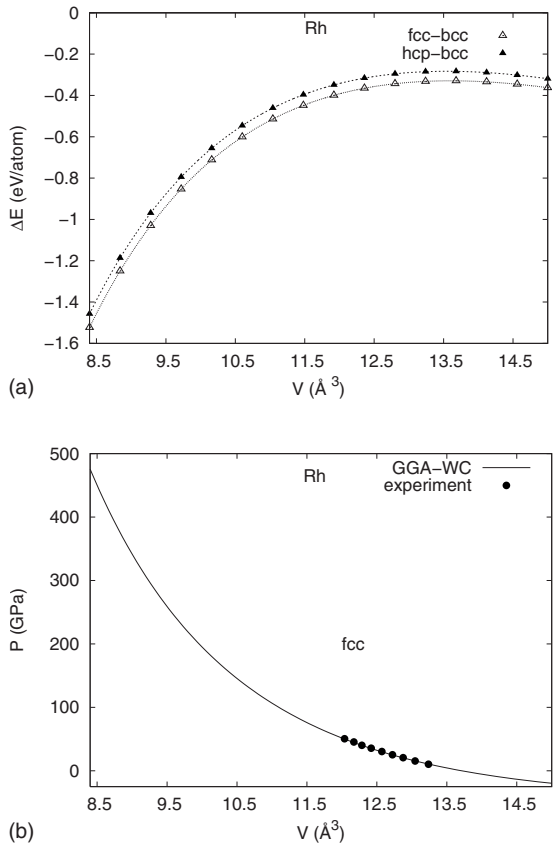

FIG. 8. *Top*: Energy differences ΔE of the fcc and hcp structures with respect to bcc in Rh as function of volume. *Bottom*: Equation of state of Rh up to $P \sim 500$ GPa compared with experimental data.[71]

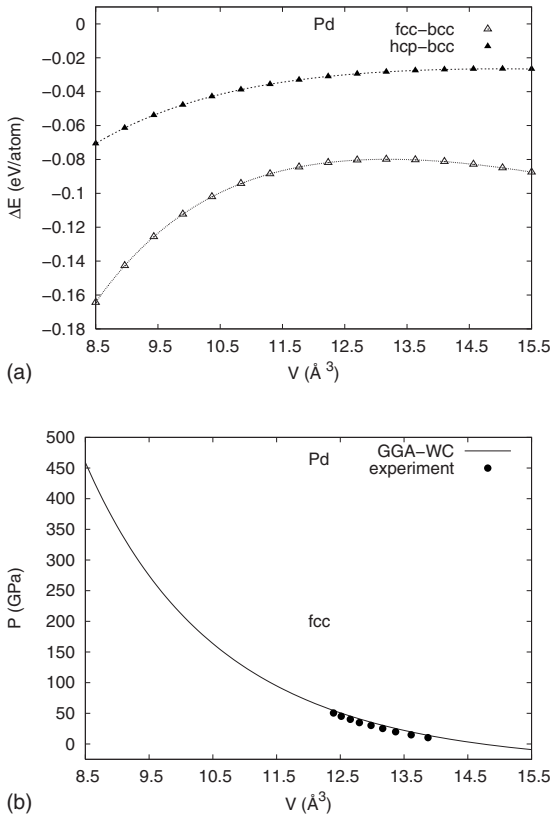

FIG. 9. *Top*: Energy differences ΔE of the fcc and hcp structures with respect to bcc in Pd as function of volume. *Bottom*: Equation of state of Pd up to $P \sim 450$ GPa compared with experimental data.[71]

are available, but in DFT theory there is no difficulty in treating Z as continuous. (In tight-binding theories of transition-metal energetics, it is common practice to treat the number of electrons per atom as continuous.) However, to save effort, we have not actually attempted to perform FP-LAPW calculations for noninteger Z, preferring to obtain the phase boundaries by simple interpolation.

To perform the interpolation, we note that at $T=0$ K the enthalpies $H \equiv E+PV$ of coexisting phases must be equal. To take an example, the hcp-bcc energy differences for Mo ($Z=42$) and Tc ($Z=43$) at $P=400$ GPa are 0.62 and −0.22 eV/atom, and the hcp-bcc volume differences are −0.14 and −0.12 Å^3/atom, so that the hcp-bcc enthalpy differences are 0.27 and −0.52 eV/atom. By linear interpolation, we estimate $Z=42.34$ as the coexistence value between bcc and hcp at 400 GPa. We have used this interpolation scheme to estimate the bcc-hcp boundary between Mo and Tc, and the hcp-fcc boundary between Ru and Rh. For the complicated region Y-Zr-Nb, we have performed interpolation only for the fcc-bcc boundary passing through the Y-Zr region; in the other cases, the boundaries have been drawn approximately by means of straight lines. The resulting generalized phase diagram is shown in Fig. 10.

IV. DISCUSSION AND CONCLUSIONS

We noted in Sec. I the general expectation that the sequence of crystal structures across a transition-metal series will be the same at high P as at low P, but that the phase boundaries should slope to the left ($dP/dZ<0$). The well-known ideas behind this expectation are that (a) the sequence of stable structures depends mainly on the band energy, i.e., the sum of single-electron energies; (b) the band energy depends mainly on the d-band densities of states in the different crystal structures, and on the number of d electrons; (c) for given atomic number Z, increase of P causes the bottom

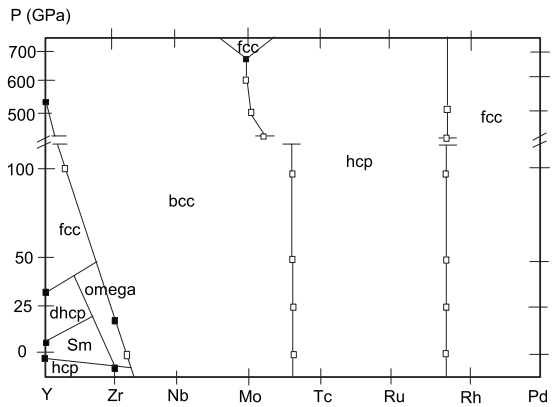

FIG. 10. Calculated zero-temperature phase diagram of the 4d transition-metals series. Solid squares correspond to phase transitions obtained directly from the FP-LAPW calculations while open squares show results obtained by interpolation (see text).

of the d band to rise with respect to the d-band centroid, so that the effective number of d electrons increases. Because of this last effect, increase of P should cause a given element to become more like its neighbor on the right. This is expected to be a stronger effect for early transition metals, since the increase of the effective number of d electrons with compression is larger for them.[18]

These expectations are confirmed most clearly by the major boundary separating bcc from more close-packed structures on the left of the phase diagram. This boundary causes Zr at rather moderate pressures to adopt the low-P structure of Nb, and Y to do the same at much higher pressures. However, the boundary separating bcc and hcp in the middle of the diagram is almost vertical up to $P \sim 100$ GPa, and it is only at much higher pressures that it slopes to the left; furthermore, it appears that Mo never adopts the low-P structure of its neighbor Tc. Similarly, the boundary between hcp and fcc on the right of the diagram is practically vertical up to $P \sim 500$ GPa.

DFT predictions of the many transitions shown by Y and Zr already give evidence that DFT provides reasonably good quantitative accuracy for the pressure dependence of band structures. The bcc-fcc transition in Mo will probably remain out of reach of experiment for some time. On the controversial question of whether the high-P transition in Mo is really bcc-fcc or bcc-hcp, our results support the former. The reason for this controversy is clearly that the hcp and fcc energies are very close to each other, so that the calculations have to be converged to high accuracy to yield reliable conclusions. We have taken pains to ensure that our prediction of bcc-fcc is robust with respect to all convergence parameters. Consequently, we believe that the small and unexpected field of fcc at high P and roughly half band filling is a real effect.

The bcc-fcc transition in Mo is relevant to the interpretation of the shock experiments mentioned in Sec. I. When this transition was first studied theoretically, the predicted transition pressure was 420 GPa,[21] which is much lower than our value of 660 GPa. At that time, it seemed likely that the transition is closely related to the transition seen in shock experiments[54] on Mo at $P \simeq 210$ GPa and an (estimated) temperature of 3100 K. Our confirmation of earlier work giving a much higher transition pressure makes it much less likely that there is a direct connection with the shock transition. The only way of maintaining this connection would be to postulate that the transition pressure decreases strongly with increasing temperature. However, our DFT calculations of phonon frequencies in the two structures[72] show that the transition pressure actually *increases* with temperature so that a direct connection with the shock transition is completely ruled out.

Turning now to detailed comparisons with experiment, we have shown that all our calculated equations of state $P(V)$ agree very closely with experiment. The sequences of stable structures with increasing pressure are always correctly predicted, where experimental data are available, but our calculations have a clear tendency to underestimate transition pressures P_t by typically ~ 10 GPa. This can be attributed to a relative shift δE of the energies of coexisting phases. Since at $T=0$ K, the enthalpies H of coexisting phases are equal, a shift of P_t is related to δE by

$$\delta E = \delta P_t((\partial H_1/\partial P)_T - (\partial H_2/\partial P)_T), \quad (1)$$

where $H_1(P)$ and $H_2(P)$ are the enthalpies of the two phases. Since $(\partial H/\partial P)_T = V$, the shift δP_t can be estimated as $\delta P_t = \delta E/(V_1 - V_2)$, where V_1 and V_2 are the coexisting volumes. Then a shift $\delta P_t = 10$ GPa equates to a ratio $\delta E/(V_1 - V_2) = 60$ meV/Å^3 atom. Taking an example, the volume change $V_1 - V_2$ at the hcp-ω transition of Zr was calculated to be 0.1 Å^3/atom, so it would require a relative shift of 6 meV/atom to account for the error in P_t. On the other hand, for the ω-bcc transition of Zr, for which $V_1 - V_2 = 0.6$ Å^3/atom, the relative shift would have to be 36 meV/atom. It is easy to see that room-temperature thermal effects are unlikely to be the cause. Estimating the vibrational free energy per atom F_{vib} as $3k_BT \ln(\hbar\bar{\omega}/k_BT)$, with $\bar{\omega}$ the geometric-mean phonon frequency, a difference $\delta\bar{\omega}$ between coexisting phases causes a relative free-energy shift $\delta F_{\mathrm{vib}} \simeq 3k_BT\delta\bar{\omega}/\bar{\omega}$. With $3k_BT = 80$ meV at room temperature, unreasonably large $\delta\bar{\omega}/\bar{\omega}$ values would be required. On the other hand, we have cited evidence (Table III) that differences between density functionals can lead to P_t shifts of order 10 GPa in the ω-bcc transition of Zr. However, there is a third possible cause, namely approximations in the implementation of DFT. We have made efforts to ensure that our FP-LAPW energies are converged to ~ 1 meV/atom with respect to plane-wave and angular-momentum cutoffs, but there remain possible linearization errors, whose size is difficult to estimate. It seems clear that such errors must be the reason for some of the very large differences between DFT predictions of P_t values. We think this explains the difference of over 200 GPa in the predicted P_t of the fcc-bcc transition in Y (Table II), because the earlier DFT work was done at a time when the treatment of semicore states was less well developed. The range of ~ 300 GPa in predicted P_t values for the high-P transition in Mo must also be attributed to implementation errors in early work.

We conclude by recalling that the present calculations on the zero-temperature (P,Z) phase diagram are intended as a prelude to the systematic mapping of the (P,T,Z) diagram, including the solid-liquid coexistence surface as a function of P and Z. In spite of major progress in the first-principles calculation of melting curves over the past 10 years,[23,73–75] the computation of the entire (P,T,Z) phase diagram is clearly a major challenge, which will need to be tackled in stages. The use of DFT to calculate harmonic vibration frequencies[76] will allow quite rapid progress at temperatures up to about one third of the melting temperature, and we have already reported systematic calculations of this kind for Fe, Ta, and Mo over a wide range of pressures.[77,78] For melting curves, several first-principles methods are available.[74,75] However, we believe it will also be valuable to make rapid and more approximate surveys using tight-binding methods, and we plan to report on this approach in the near future.

ACKNOWLEDGMENTS

The work was supported by EPSRC-GB Grant No. EP/C534360, which is 50% funded by DSTL(MOD). The work was conducted as part of a EURYI scheme award to D.A. as provided by EPSRC-GB.

[1] J. Friedel, in *The Physics of Metals*, edited by J. M. Ziman (Cambridge University Press, London, 1969).
[2] J. C. Duthie and D. G. Pettifor, Phys. Rev. Lett. **38**, 564 (1977).
[3] V. Heine, Phys. Rev. **153**, 673 (1967).
[4] C. Cazorla, M. J. Gillan, S. Taioli, and D. Alfè, J. Chem. Phys. **126**, 194502 (2007).
[5] S. Taioli, C. Cazorla, M. J. Gillan, and D. Alfè, Phys. Rev. B **75**, 214103 (2007).
[6] D. Errandonea, Physica B (Amsterdam) **357**, 356 (2005).
[7] M. Ross, D. Errandonea, and R. Boehler, Phys. Rev. B **76**, 184118 (2007).
[8] Y. Ding, R. Ahuja, J. Shu, P. Chow, W. Luo, and H.-K. Mao, Phys. Rev. Lett. **98**, 085502 (2007).
[9] We refer to a phase diagram in which atomic number Z is one of the variables as a "generalized phase diagram," following B. Johansson and A. Rosengren, Phys. Rev. B **11**, 2836 (1975).
[10] O. K. Andersen, Phys. Rev. B **12**, 3060 (1975).
[11] D. D. Koelling and G. O. Arbman, J. Phys. F: Met. Phys. **5**, 2041 (1975).
[12] D. D. Koelling and B. N. Harmon, J. Phys. C **10**, 3107 (1977).
[13] D. Singh, *Planewaves, Pseudopotentials and the LAPW Method* (Kluwer, Boston, 1994).
[14] Z. Wu and R. E. Cohen, Phys. Rev. B **73**, 235116 (2006).
[15] F. Tran, R. Laskowski, P. Blaha, and K. Schwarz, Phys. Rev. B **75**, 115131 (2007).
[16] L. Brewer, in *Batelle Institute Materials Science Colloquia*, edited by P. S. Rudman, J. Stringer, and R. I. Jaffee (McGraw-Hill, New York, 1967), pp. 39–67.
[17] P. Söderlind, R. Ahuja, O. Eriksson, J. M. Wills, and B. Johansson, Phys. Rev. B **50**, 5918 (1994).
[18] D. G. Pettifor, J. Phys. F: Met. Phys. **7**, 613 (1977).
[19] N. W. Dalton and R. A. Deegan, J. Phys. C **2**, 2369 (1969).
[20] F. Ducastelle and F. Cyrot-Lackmann, J. Phys. Chem. Solids **32**, 285 (1971).
[21] J. A. Moriarty, Phys. Rev. B **45**, 2004 (1992).
[22] A. K. McMahan, Physica B (Amsterdam) **139**, 31 (1986).
[23] A. B. Belonoshko, S. I. Simak, A. E. Kochetov, B. Johansson, L. Burakovsky, and D. L. Preston, Phys. Rev. Lett. **92**, 195701 (2004).
[24] D. G. Pettifor, J. Phys. C **3**, 367 (1970).
[25] D. G. Pettifor, in *Metallurgical Chemistry*, edited by O. Kubashewski (Her Majesty's Stationery Office, London, 1972).
[26] H. L. Skriver, Phys. Rev. B **31**, 1909 (1985).
[27] D. Vanderbilt, Phys. Rev. B **41**, 7892 (1990).
[28] P. E. Blöchl, Phys. Rev. B **50**, 17953 (1994).
[29] G. Kresse and D. Joubert, Phys. Rev. B **59**, 1758 (1999).
[30] H. J. Monkhorst and J. D. Pack, Phys. Rev. B **13**, 5188 (1976).
[31] P. Blaha, K. Schwarz, G. K. Madsen, D. Kvasnichka, and J. Luitz, *WIEN2k: An Augmented Plane Wave Plus Local Orbital Program for Calculating Crystal Properties* (Technical University of Vienna, Vienna, 2001).
[32] J. P. Perdew, K. Burke, and M. Ernzerhof, Phys. Rev. Lett. **77**, 3865 (1996).
[33] Y. Wang and J. P. Perdew, Phys. Rev. B **44**, 13298 (1991).
[34] P. S. Svendsen and U. von Barth, Phys. Rev. B **54**, 17402 (1996).
[35] D. M. Ceperley and B. J. Alder, Phys. Rev. Lett. **45**, 566 (1980).
[36] R. S. Hixson and J. N. Fritz, J. Appl. Phys. **71**, 1721 (1992).
[37] F. Birch, Phys. Rev. **71**, 809 (1947).
[38] The dhcp and αSm structures are both variations of close packing. Whereas hcp and fcc have the sequences ABAB... and ABCABC..., dhcp goes ABACABAC... and αSm goes ABCBCACAB... .
[39] Y. K. Vohra, H. Olijnik, W. Grosshans, and W. B. Holzapfel, Phys. Rev. Lett. **47**, 1065 (1981).
[40] W. A. Grosshans and W. B. Holzapfel, Phys. Rev. B **45**, 5171 (1992).
[41] B. Johansson and A. Rosengren, Phys. Rev. B **11**, 2836 (1975).
[42] S. Lei, D. A. Papaconstantopoulos, and M. J. Mehl, Phys. Rev. B **75**, 024512 (2007).
[43] J. Melsen, J. M. Wills, B. Johansson, and O. Eriksson, Phys. Rev. B **48**, 15574 (1993).
[44] Z. P. Yin, S. Y. Savrasov, and W. E. Pickett, Phys. Rev. B **74**, 094519 (2006).
[45] Y. Zhao, J. Zhang, C. Pantea, J. Qian, L. Daemen, P. Rigg, R. Hixson, G. Gray, Y. Yang, L. Wang, Y. Wang, and T. Uchida, Phys. Rev. B **71**, 184119 (2005).
[46] H. Xia, S. J. Duclos, A. L. Ruoff, and Y. K. Vohra, Phys. Rev. Lett. **64**, 204 (1990).
[47] S. A. Ostanin and V. Yu. Trubitsin, Phys. Rev. B **57**, 13485 (1998).
[48] I. Schnell and R. C. Albers, J. Phys.: Condens. Matter **18**, 1483 (2006).
[49] F. Jona and P. M. Marcus, J. Phys.: Condens. Matter **15**, 5009 (2003).
[50] J. E. Garcés, G. B. Grad, A. F. Guillermet, and S. J. Ferco, J. Alloys Compd. **289**, 1 (1999).
[51] G. B. Grad, P. Blaha, J. Luitz, K. Schwarz, A. Fernandez Guillermet, and S. J. Sferco, Phys. Rev. B **62**, 12743 (2000).
[52] T. Kenichi and A. K. Singh, Phys. Rev. B **73**, 224119 (2006).
[53] J. Donohue, *The Structures of the Elements* (Wiley, New York, 1974).
[54] R. S. Hixson, D. A. Boness, J. W. Shaner, and J. A. Moriarty, Phys. Rev. Lett. **62**, 637 (1989).
[55] F. Jona and P. M. Marcus, J. Phys.: Condens. Matter **17**, 1049 (2005).
[56] N. E. Christensen, A. L. Ruoff, and C. O. Rodriguez, Phys. Rev. B **52**, 9121 (1995).
[57] J. C. Boettger, J. Phys.: Condens. Matter **11**, 3237 (1999).
[58] P. Söderlind, R. Ahuja, O. Eriksson, B. Johansson, and J. M. Wills, Phys. Rev. B **49**, 9365 (1994).
[59] E. A. Smirnova, R. Ahuja, Y. Kh. Vekilov, B. Johansson, Y. K. Vohra, and I. A. Abrikosov, Phys. Rev. B **66**, 024110 (2002).
[60] L. Hedin and B. Lundqvist, J. Phys. C **4**, 2064 (1971).
[61] J. P. Perdew and A. Zunger, Phys. Rev. B **23**, 5048 (1981).
[62] U. von Barth and L. Hedin, J. Phys. C **5**, 1629 (1972).
[63] M. I. McMahon and R. J. Nelmes, Chem. Soc. Rev. **35**, 943 (2006).
[64] H. Cynn, J. E. Klepeis, C.-S. Yoo, and D. A. Young, Phys. Rev. Lett. **88**, 135701 (2002).
[65] *Structure Data of Elements and Intermetallic Phases*, Landolt-Börnstein, New Series, Group III, Vol. 14, Pt. A, edited by K.-H. Hellwege and A. M. Hellwege (Springer, Berlin, 1988).
[66] C. Kittel, *Introduction to Solid State Physics* (Wiley, New York, 1976).
[67] V. A. Finkel, M. I. Palatnik, and G. P. Kovtun, Phys. Met. Metallogr. **32**, 231 (1971).
[68] J. X. Zheng-Johansson, O. Eriksson, and B. Johansson, Phys. Rev. B **59**, 6131 (1999).
[69] E. A. Perez-Albuerne, K. F. Forsgren, and H. G. Drickamer, Rev. Sci. Instrum. **35**, 29 (1964).

[70] H. K. Mao, P. M. Bell, J. Shaner, and D. J. Steinberg, J. Appl. Phys. **49**, 3276 (1978).
[71] M. H. Rice, R. G. McQueen, and J. H. Walsh, Solid State Phys. **6**, 1 (1958).
[72] C. Cazorla and M. J. Gillan (unpublished).
[73] D. Alfè, M. J. Gillan, and G. D. Price, Nature (London) **401**, 462 (1999).
[74] D. Alfè, M. J. Gillan, and G. D. Price, J. Chem. Phys. **116**, 6170 (2002).
[75] D. Alfè, G. D. Price, and M. J. Gillan, J. Phys. Chem. Solids **65**, 1573 (2004).
[76] P. Souvatzis and O. Eriksson, Phys. Rev. B **77**, 024110 (2008).
[77] L. Vočadlo, D. Alfè, M. J. Gillan, I. G. Wood, J. P. Brodholt, and G. D. Price, Nature (London) **424**, 536 (2003).
[78] C. Cazorla, M. J. Gillan, S. Taioli, and D. Alfè, J. Phys.: Condens. Matter (to be published).